IEEE Access
Multidisciplinary ⋮ Rapid Review ⋮ Open Access Journal

Received December 7, 2018, accepted December 12, 2018, date of publication December 18, 2018,
date of current version January 7, 2019.

Digital Object Identifier 10.1109/ACCESS.2018.2887233

Design and Experimental Research of Movable Cable-Driven Lower Limb Rehabilitation Robot

YUPENG ZOU[1], NUO WANG[1], XINQING WANG[1], HUIZI MA[2], AND KAI LIU[1]
[1]College of Mechanical and Electronic Engineering, China University of Petroleum, Qingdao 266580, China
[2]College of Mathematics and System Science, Shandong University of Science and Technology, Qingdao 266590, China

Corresponding author: Yupeng Zou (zouyupeng@upc.edu.cn)

This work was supported in part by the National Natural Science Foundation of China under Grant 51705534, in part by the Fundamental Research Funds for the Central Universities under Grant 18CX02085A and Grant 18CX02088A, in part by the Key Scientific and Technological Innovation Project of Shandong Provincial under Grant 2017CXGC0902, and in part by the Shandong Provincial Natural Science Foundation under Grant ZR2016EEB12.

ABSTRACT Aiming at solving the problems of the existing lower limb rehabilitation robots on aspects of configuration limitations, human–machine compatibility, gravity compensation, and multimodal rehabilitation, a movable cable-driven lower limb rehabilitation robot (MCLR) is proposed in this paper, which can realize the gait training and walking training in passive mode, initiative mode, and assistive mode. First, the structure and working principle of MCLR is introduced. The traction type is further optimized. Second, the key control problems of the passive force servo system are analyzed in detail. In order to improve the loading accuracy and speed during the initiative training, the dynamic model of the cable-driven unit is established. Based on this model, an active force control strategy is proposed. Finally, the speed control strategy and the active force control strategy are studied experimentally. The experimental results show that the speed servo system has good tracking ability, which can meet the requirements of the passive rehabilitation. The active force control strategy can significantly improve the loading accuracy and the dynamic performance of the force servo system. The force servo system has good tracking ability in the normal rehabilitation frequency band, which can meet the requirements of the initiative rehabilitation.

INDEX TERMS Lower limb rehabilitation, cable driven, configuration Optimization, active force control, passive force servo system.

I. INTRODUCTION

At present, the growth trend of aging population is particularly evident. The *World Population Outlook* released by the United Nations shows that there were 962 million people aged 60 and over worldwide in 2017. By 2050, the aging population will be more than double that of today, and by 2100 it will be more than triple that of today, reaching 3.1 billion [1]–[3]. The incidence of cardiovascular diseases (especially stroke) and nervous system diseases is very high in the elderly. These diseases will lead to lower limb hemiplegia and even paraplegia. In addition, the number of patients with lower extremity dyskinesia caused by natural disasters, accidents and other reasons is also increasing. The patients with lower extremity dyskinesia will suffer psychological trauma which may lead to pessimism and depression easily. Their daily life is further affected. Research shows that the scientific and correct rehabilitation plays an important role in the recovery of motor function. Therefore, how to restore the normal motor ability of patients with lower extremity dyskinesia to the greatest extent is a difficult task in the whole rehabilitation field [4], [5].

In terms of the robot configuration, the lower limb rehabilitation robots can be roughly divided into the exoskeleton-type (like the Lokomat) and the footpad-type (like the G-EO system) [6]–[8]. The existing lower limb rehabilitation robots have the following limits.

1) *Configuration Limitations:* The exoskeleton-type robots have low stiffness and large motion accumulative error for the serial structure. The interaction force is difficult to control due to the large inertia. The footpad-type robots are difficult to achieve single-joint rehabilitation, and the pedals will produce additional reaction forces act on the lower limbs.

2) *Poor Human-Machine Compatibility:* Limited by the degree of freedom of the robot, especially the exoskeleton-type rehabilitation robot, there are motion differences and interference between the lower limb and the exoskeleton.

2169-3536 © 2018 IEEE. Translations and content mining are permitted for academic research only.
Personal use is also permitted, but republication/redistribution requires IEEE permission.
See http://www.ieee.org/publications_standards/publications/rights/index.html for more information.

The robot cannot follow the lower limb synchronously which makes patients uncomfortable [9].

3) *Gravity Compensation:* The existing lower limb rehabilitation robots need to overcome the gravity of the components and the patient's body in the rehabilitation process, which leads to the large and complex mechanism, the greater energy consumption, and poor motion accuracy, etc. [10], [11].

4) *Monotonous Training Modes:* In different rehabilitation stages, the rehabilitation robots need to achieve various forms of force/position control according to different rehabilitation modes and stages. Most robots can achieve position control easily, but few robots can achieve complex force control. For the existing lower limb rehabilitation robots, it is difficult to implement gait training and walking training with passive, initiative and assistive mode on one lower limb rehabilitation robot.

In the cable-driven mechanisms, the flexible cables are used to replace the traditional rigid links as the transmission elements [12]. Compared with the traditional rigid mechanisms, the cable-driven mechanisms have higher load-weight ratio, higher speed-accuracy ratio and adjustable stiffness. These unique performance advantages make the cable-driven mechanisms have broad application prospects in the rehabilitation. Agrawal *et al.* designed a cable-driven arm exoskeleton (CAREX) and a cable-driven active leg exoskeleton (C-ALEX) for the human limb rehabilitation. The advantages of the cable-based exoskeletons are that they have a simpler structure, add minimal inertia to the human limbs, and do not require precise joint alignment [13], [14]. However, the structure nature of the cable-driven exoskeletons is still the serial form. The trajectory control precision is still severely affected by the layout form of the cuffs which is determined by the limbs parameters. In addition, it is difficult to simulate the complex mechanics characteristic of limbs using the serial cable-driven robots. A 3-DOFs wire-based upper limb rehabilitation robot NeReBot and a 5-DOFs wire-based upper limb rehabilitation robot MariBot were developed at the University of Padua, Italy. One fundamental difference in the architecture of their design was that NeReBot and MariBot were all typical incompletely restrained positioning mechanisms. The robots cannot function properly without the external forces (for example, gravitation and spring force). For this feature, the training space is limited and the training mode is single [15], [16]. Irrespective of the external forces, one disadvantage of the cable-driven mechanisms is that the cable-driven mechanisms need redundant actuators to ensure the cables be in tension during the motion control. The STRING-MAN, developed by Surdilovic, was a completely restrained positioning mechanisms. In order to realize the 6-DOFs posture control, the number of applied wires was one higher than the number of the controlled DOFs [17]. Alamdari *et al.* designed a cable-driven articulated gait rehabilitation system (ROPES) and a parallel articulated cable exercise robot (PACER). These two robots examined the viability of a light-weight and reconfigurable hybrid (articulated-multibody and cable) robotic system for rehabilitation [18], [19].

Despite all the advantages listed for the cable-driven mechanisms, using cables in the robot structure introduces a new challenge, which stems from the fact that cables can only apply tension forces [20], [21]. Thus controller design of the cable-driven robot is more difficult than that of the conventional parallel robots and serial robots [22], [23]. According to the rehabilitation modes, the cable-driven rehabilitation robot needs to switch between the position control and the force control.

The existing motion controllers of the cable-driven robots can be classified into two categories [24], the ones that are formed in the task space (TS) and the others that are designed in the cable space (CS). Some latest modeling and control methods can be introduced to the motion control of the cable-driven robots [25]–[28].

During the initiative training process, the cable-driven rehabilitation robot is a typical passive force servo system. The control strategy design of the passive force servo system should consider two aspects: one is to improve the tracking ability, and the other is to restrain the disturbance (the surplus force) [29]. The current research emphasis is focused on reducing the surplus force. To ensure the stability, the force servo system is generally corrected by the PID controller. However, the PID controller can only provide limited phase compensation, leading to an unsatisfactory dynamic quality [30]. To improve the dynamic performance, the modern control theory can be adopted, such as the neural network control and the adaptive control [31], [32]. In order to suppress the surplus force and improve the loading accuracy, the active compensation method is the most popular approach which suppresses the surplus force through control strategies (control compensation method). Wang et al. adopted the speed synchronization compensation control. The basic idea was to introduce a speed closed loop on the basis of the force closed loop of the original loading system to keep the loading motor and the carrying unit motion synchronously, so as to eliminate the surplus force [33]. Fang *et al.* proposed a compensation method based on the disturbance observer. This method used a dual-loop structure: a disturbance observer was designed for the inner loop, and the controller was designed for the outer loop based on the nominal model after correction [34]. In addition, intelligent controls, such as robust control, composite control strategy based on RBF, composite control strategy based on CMAC, have been applied in solving the surplus force [35]–[37].

The remainder of the paper is organized as follows: In Section 2, the structures of the MCLR and the CDU are introduced; the specific rehabilitation process and advantages of using MCLR to realize gait training and walking training are expounded further. By analyzing the relationship between PCDM's workspace and the limb posture, the traction type of the MCLR is determined in Section 3. In Section 4, the key control problems of the passive force servo system are

explicated in detail. Section 5 shows the design of the active force control strategy. The speed control strategy and the active force control strategy are studied experimentally in Section 6. Finally, conclusions are drawn and further work is forecasted.

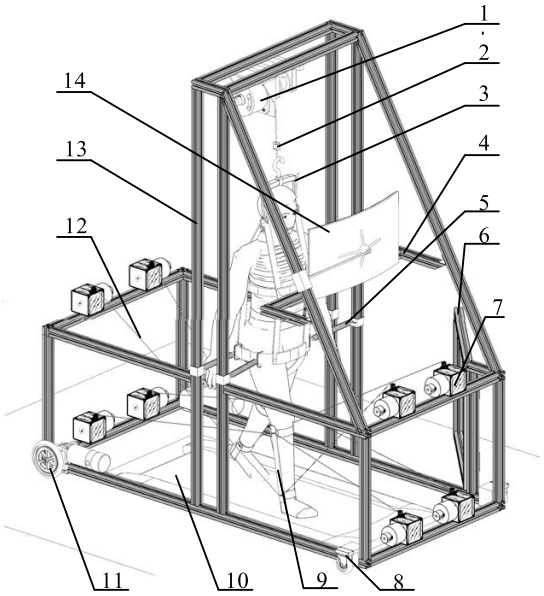

FIGURE 1. Movable cable-driven lower limb rehabilitation robot: 1-Body weight support system, 2-Tension sensor, 3-Safety belt, 4-Safety handrail, 5-Spring, 6-Passageway, 7-Cables-driven unit, 8-Universal wheel, 9-Leg support plate, 10-Treadmill, 11-Rear driving wheel, 12-Cable, 13-Support frame, 14-Human machine interaction device.

II. MCLR & CDU

A. WORKING PRINCIPLE OF MCLR

The structure of MCLR is shown in Fig. 1. The lower limb rehabilitation robot is 2.1 meters long, 1.0 meters wide and 2.3 meters high. In the MCLR, the body weight support system (BWS) is mounted on the top of the support frame. It can provide different gravity-loss effects according to the different rehabilitation modes and stages. By cooperating with the CDUs, the BWS can coordinate the lower limbs and trunk to ensure the posture's accuracy and the patient's safety.

There are four springs between the vertical beams and the wrist of the patient. The springs can fix the relative position of the patient's lower body within a certain range to ensure the stability of the human body during the rehabilitation training.

The human machine interaction device can be used to monitor the rehabilitation status in real time. In addition, the introduction of training games can also improve the effect and interest of rehabilitation.

The MCLR contains two sets of 1R2T (1 rotation and 2 translation) Parallel Cable-Driven Mechanisms (PCDM). Each PCDM, containing four CDUs, can realize 3-DOF movement of the lower limb in the sagittal plane. The CUDs are installed on four crossbeams corresponding to the sagittal plane of each side of the lower limb, and can move left and right according to the patient's body shape to ensure that the CDUs and the lower limb are in the same sagittal plane. As shown in Fig. 1, the ankle joints are drawn by the four CDUs attached on the upper crossbeams, and the knee joints are drawn by the four CDUs attached on the lower crossbeams.

The chassis is fitted with two universal wheels and two driving wheels. Changing the motion state of the movable chassis, the patient can do gait training on the treadmill or do walking training on the ground. When the chassis is fixed, the gait training can be realized by the coordination of the CDUs and the treadmill. When the chassis moves, the walking training can be realized by the coordination of the CDUs and the movable chassis.

Depending on the training modes, the control mode of CDU can be switched between speed servo control and force servo control. All the CDUs coordinate with each other, and ultimately achieve the passive training, initiative training and assistive training.

The advantages of the MCLR are shown in the following aspects.

(i) *Configuration Advantages:* The movement of the cables is more flexible than the traditional rigid pairs. Thus, compared with the footpad-type robots, MCLR has larger workspace at the same boundary dimensions, which ensures the implementation of single-joint rehabilitation. Compared with the exoskeleton-type robots, MCLR is essentially a parallel mechanism, which has the merits of high structural stiffness, small motion inertia, and high kinematic precision. What's more, the training compliance could be improved significantly by adjusting the cable internal tension.

(ii) *Good Human-Machine Compatibility:* As a kind of transmission component, the cables for rehabilitation have good flexibility to avoid rigid impact. In addition, the contact area or the number of the contact points between the human and the robot is small. This characteristic can reduce the man-machine motion interference effectively.

(iii) *No Gravity Compensation:* Owing to the lightness of the cable, the overall mass of the rehabilitation robot and the energy consumption are reduced and pipeline system safety and the dynamic performance of the system is improved.

(iv) *Multimodal Rehabilitation:* Through the coordination of modular CDUs and the movable chassis, MCLR can realize the gait training and walking training in passive mode, initiative mode and assistive mode. Changing the layout of the CDUs, more other forms of rehabilitation training can be implemented.

B. STRUCTURE OF CDU

Fig. 2 illustrates the composition of the CDU. The CDU adopts modular design. Adopting this method will be in favor of the configuration reconstruction and expending service functions. In the CDU, a torque motor is used to drive the roller directly for its features of low speed and high torque. Under the constraints of the screw, the roller executes screw motion. This design ensures that the cable winds around the

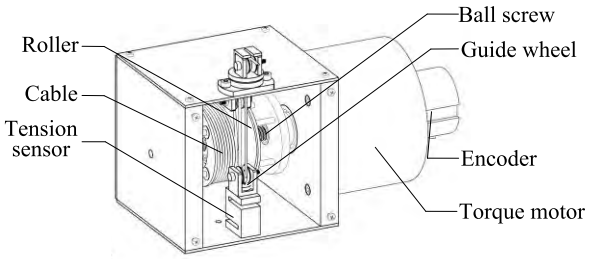

FIGURE 2. Cable-driven unit.

roller in an orderly way. A tension sensor is fixed on the bottom of the frame, and a guide wheel is located on the opposite part of the tension sensor. The motion direction of the cable changes 180° after passing through this guide wheel. The tension of the sensor is twice as much as the tension of the cable. This can reduce the influence of the electromagnetic noise and the inertia on the measurement results. An increment encoder is located on the motor, and the encoder's readings are used to determine the cable elongation. The pose state and localization of the lower limbs can be further determined.

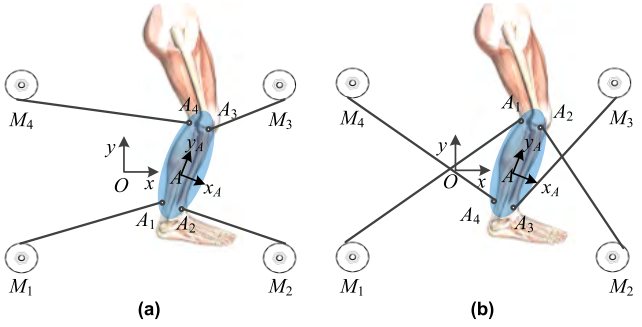

FIGURE 3. Traction types of 1R2T PCDM. (a) Traction type I. (b) Traction type II.

III. CONFIGURATION DESIGN OF MCLR

As shown in Fig. 3, the 1R2T PCDM has two traction types. In different traction types, the moving platform $A_1A_2A_3A_4$ has different workspaces. Even in the same traction type, different sizes of $A_1A_2A_3A_4$ and $M_1M_2M_3M_4$ can lead to different workspaces. It's obvious that the workspace of PCDM can be effectively expanded with the increasing of the distance between the driving points M_i. However, the overall size of MCLR will increase.

In addition, in traction type I, the height of the driving point M_1 and M_2 are lower than that of the walking platform. The motion function of MCLR cannot be realized. As for traction type II, the driving point M_1 and M_2 can be designed higher than the walking platform so as to realize the motion function of MCLR. The traction type II should be selected preferentially. To achieve complete gait training, the workspace of MCLR can be further enlarged by optimizing the position of the traction points A_i.

MCLR is expected to achieve passive rehabilitation, assistive rehabilitation and initiative rehabilitation.

In the passive training process, the CDUs take the initiative to drive the shank in accordance with the natural gait. The four cables in PCDM need to meet the static balance conditions at any time. Too many traction points will increase the difficulty in solving the cable tensions.

In the initiative training process, the CDUs passively follow the active movement of lower limbs and exert a desired resultant force on the shank. Excessive traction points will reduce the force control accuracy, and additional torque may even generate.

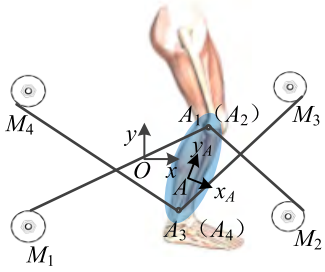

FIGURE 4. The optimized configuration of MCLR.

Synthesizes the above questions, the configuration of MCLR is shown in Fig. 4. As shown in Fig. 4, there are only two traction points on the shank. Two cable tensions form a plane intersection force system at the traction points. With fewer traction points, the difficulty in solving the cable tensions will decrease and the resultant force control accuracy will be improved.

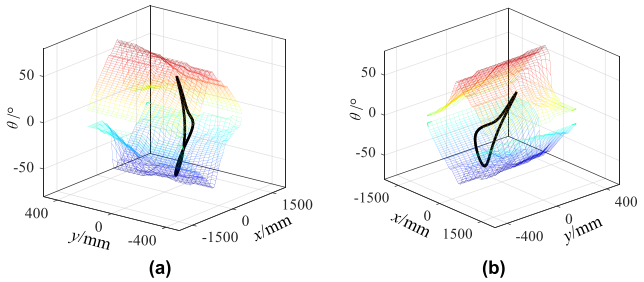

FIGURE 5. Relationship between the workspace of MCLR and the position/posture of the shank.

The relationship between the workspace of MCLR and the position/posture curve of the shank is shown in Fig. 5. In the shank's position/posture curve, the horizontal coordinates x and y represent the trajectory of the reference point A, and the θ axis represents the angle of the shank at different reference points. The entire position/posture curve has been enveloped in the workspace, and there is enough margin to meet the rehabilitation requirements of patients with different heights. The robot configuration shown in Fig. 4 can meet the training needs.

IV. CONTROL STRATEGIES

A. KEY CONTROL PROBLEMS ANALYSIS

In the passive or assistive-passive mode, the controlled variable of MCLR is the drawing velocity or displacement. MCLR is a typical speed servo system. This requires the actual cable drawing velocity to follow the desired drawing velocity accurately. Because the open-loop transfer function of the DC motor speed servo system is a zero-type system, the speed servo system can easily achieve stable, fast and accurate results with ordinary PI controller. Therefore, the detailed analysis about the speed servo control strategy is not carried out in this paper.

In the initiative or assistive-initiative mode, the controlled variable of MCLR is the resultant force of the cable tensions. MCLR is a typical force servo system. This requires the resultant force loaded on the shank to follow the desired force. According to the motion state of the bearing object, the force servo system can be divided into the active force servo system (active loading) and the passive force servo system (passive loading) [38].

The active loading means that the bearing object (lower limb) remains fixed and the loading object (cable-driven unit) applies force on it according to the input. The effectiveness of the active force control strategy could be considered as the main factor in the active force servo system.

The passive loading means that the bearing object does initiative motion; the loading object follows the movements of the bearing object and exerts a force on it according to the motion state. The loading effect is affected by the control signal of the loading object and the movement disturbances of the bearing object.

During the initiative rehabilitation process, the lower limbs do initiative motion and MCLR exerts the resultant force passively. For each CDU, it's a typical passive force servo system. To design the control strategy of the passive loading, the following aspects should be considered.

(a) To improve the response speed and precision of the force control, the active force control strategy should be designed. In addition, the improvement of mechanical structure can also improve the dynamic performance.

(b) The redundant force caused by the lower limb's initiative motion is a special problem in the passive force servo system. It will seriously affect the loading accuracy. How to minimize the negative impact of the movement disturbance is also a key problem in the design of the passive force servo system.

In conclusion, for the passive force servo system, in addition to the active force control strategy, the disturbance compensator needs to be imported into the disturbance channel. The study of the active force control strategy is the basis and premise to study the control strategy of the passive loading. Aiming at the above problems, this paper will focus on designing the active force control strategy.

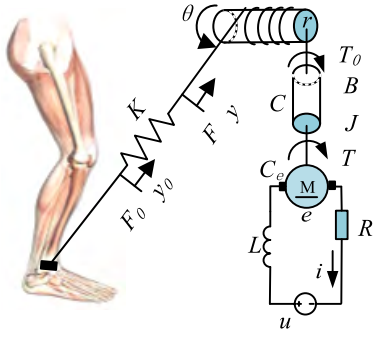

FIGURE 6. Mechanism model of cable driven unit.

B. DYNAMIC MODEL OF CDU

According to the composition and characteristics of the CDU shown in Fig. 2, the mechanism model can be described in the form shown in Fig. 6.

Compared with the rigid transmission, the cable can only be tensioned and cannot be compressed. When running normally, the cable must be always in a tension state. Generally, the cable is simplified as ''mass-spring-damping'' model. Considering that the cable used in the MCLR is light in mass and less in internal friction, the influence of the mass and the damping of the flexible cable can be negligible in the mechanism model. The cable is simplified as a spring K. In the CDU's mechanism model, the meaning of each parameter is shown in Table 1.

TABLE 1. Parameters meaning of the CDU model.

u	Motor armature voltage
L	Motor armature circuit inductance
R	Motor armature circuit resistance
e	Motor armature back EMF
C_e	Motor back EMF constant
i	Motor armature current
C_m	Motor torque constant
T	Motor driving torque
r	Radius of roller
θ	Angular displacement of the roller
F	Internal tension of cable
T_0	External load torque of motor
F_0	External tension of cable
K	Stiffness of cable
y	Linear displacement of cable on the roller
J	Equivalent moment of inertia of the roller and the motor rotor
y_0	Linear displacement of lower limb
B	Equivalent viscous friction coefficient of the roller and the motor rotor

According to Darren Bell principle, the torque balance equation of the roller and the motor rotor can be written by

dynamic and static method as

$$T - T_0 = J\ddot{\theta} + B\dot{\theta} \tag{1}$$

where $T = C_m i$.

The armature circuit equation of DC torque motor is

$$L\frac{di}{dt} + Ri + e = u \tag{2}$$

where $e = C_e\dot{\theta}$.

The cable is simplified as a ''spring'', and its force balance equation is

$$F = K(y - y_0) \tag{3}$$

Besides,

$$T_0 = Fr \tag{4}$$

$$y = \theta r \tag{5}$$

The open-loop model block diagram of the cable-driven loading system is shown in Fig. 7, which can be obtained by Laplace transformation of equation (1) ∼ (5).

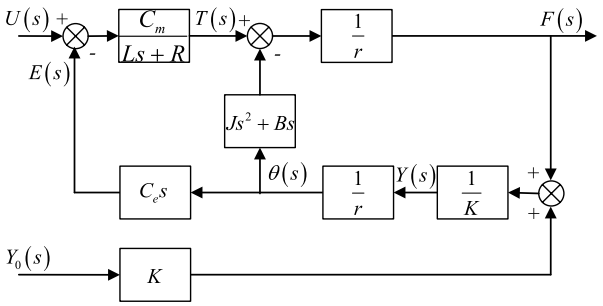

FIGURE 7. Block diagram of cable-driven loading system.

As can be seen from Fig. 7, there are two inputs that affect the output F of the cable-driven loading system. One is the motor armature voltage u, the other is the position disturbance y_0 caused by the patient's initiative motion. When the patient does not do initiative motion ($\dot{y}_0 = 0$), the cable-driven loading system is an active force servo system; when the patient does initiative motion ($\dot{y}_0 \neq 0$), the cable-driven loading system is a passive force servo system.

Based on Fig. 7, considering the influence of the bearing object's motion, the mathematical model of the cable-driven loading system is

$$F(s) = M_1(s)U(s) - M_2(s)Y_0(s) \tag{6}$$

where,

$$M_1(s) = \frac{KC_m r}{JLs^3 + (JR + BL)s^2 + (C_m C_e + BR + Lr^2k)s + kRr^2},$$

$$M_2(s) = \frac{Js^3 + (JR + BL)s^2 + (C_m C_e + BR)s}{JLs^3 + (JR + BL)s^2 + (C_m C_e + BR + Lr^2k)s + kRr^2}.$$

TABLE 2. Normal values of the CDU parameters.

Parameter	value	Parameter	value
R/Ω	10.9	$J/(\mathrm{Kg\cdot m^2})$	0.00165
L/H	0.0125	r/m	0.0275
$C_e/(\mathrm{V\cdot(rad/s)^{-1}})$	1.04	$B/(\mathrm{N\cdot m\cdot s\cdot rad^{-1}})$	0.01
$C_m/(\mathrm{N\cdot m\cdot A^{-1}})$	0.955	$K/(\mathrm{N\cdot m^{-1}})$	1×10^5

$M_1(s)$ is the transfer function from the input voltage u to the output F. It's the transfer function of the forward channel. $M_2(s)$ is the transfer function from the input disturbance y_0 to the output redundant force F. It's the transfer function of disturbance channel. The nominal values of each parameter in the CDU model are shown in Table 2.

C. INFLUENCE FACTORS ANALYSIS OF NATURAL FREQUENCY CHARACTERISTICS

The natural frequency characteristics of the cable-driven loading system are influenced by factors such as characteristics of the motor, structural characteristics of the CDU, and the characteristics of the cable. The impact analysis of these parameters can provide the basis for the structure optimization.

1) INFLUENCE OF EQUIVALENT MOMENT OF INERTIA J

The bode diagram of the forward channel transfer function $M_1(s)$ with different equivalent moment of inertia is shown in Fig. 8. It can be seen from the diagram that reducing the equivalent moment of inertia J can improve the system's traversing frequency and response speed.

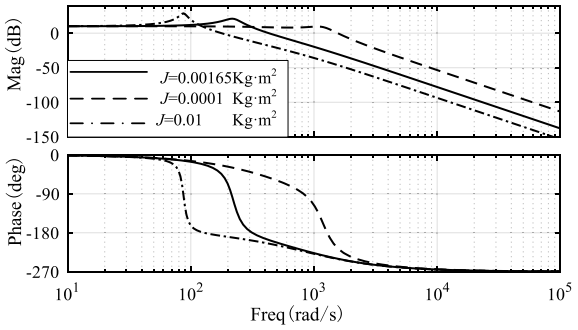

FIGURE 8. Frequency characteristic of forward channel with different equivalent moment of inertia.

2) INFLUENCE OF CABLE STIFFNESS K

The bode diagram of the forward channel transfer function $M_1(s)$ with different cable stiffness is shown in Fig. 9.

It can be seen from the diagram that increasing the stiffness can increase the system's traversing frequency, but the stability of the system will be affected. Therefore, the response speed and stability should be considered comprehensively in selecting the cable's stiffness K.

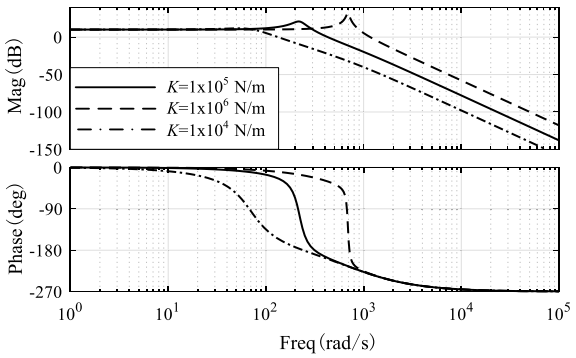

FIGURE 9. Frequency characteristic curves of forward channel with different cable stiffness.

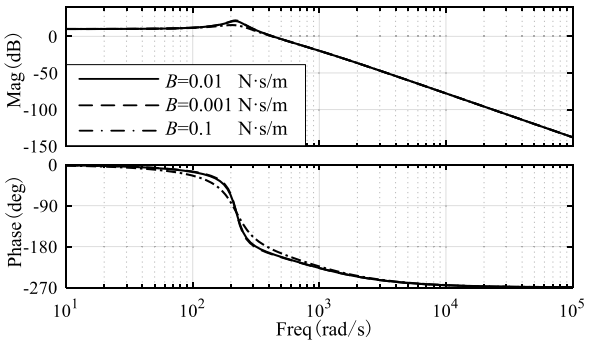

FIGURE 10. Frequency characteristic curves of forward channel with different equivalent viscous friction coefficient.

3) INFLUENCE OF EQUIVALENT VISCOUS FRICTION COEFFICIENT *B*

The bode diagram of the forward channel transfer function $M_1(s)$ with different equivalent viscous friction coefficient is shown in Fig. 10. It can be seen from the diagram that the equivalent viscous friction coefficient B has little effect on the forward channel.

D. FORWARD CHANNEL CHARACTERISTIC ANALYSIS

The dynamic characteristics of the forward channel will have an important impact on the effect of cable-driven force servo system, and directly determine the tracking ability of force command. The dynamic characteristics analysis of the forward channel transfer function $M_1(s)$ is an essential premise to determine the force control strategy.

$M_1(s)$ indicates the relationship between the input voltage u and the output force F without disturbance. Rearrange the transfer function $M_1(s)$ as follows.

$$M_1(s) = \frac{K_1}{(\frac{s}{\omega_{d1}} + 1)(\frac{s^2}{\omega_{d2}^2} + 2\xi_d \frac{s}{\omega_{d2}} + 1)} \tag{7}$$

According to equation (7), the denominator of the forward channel's transfer function can be decomposed into a first-order inertia link and a second-order oscillation link. As there is no integrating link in the denominator, $M_1(s)$ is a typical zero-type system. According to the parameters in Table 2 and equation (7), the gain $K_1 = 1.2733 \times 10^8$; the turning frequency of the system in the first-order inertial link $\omega_{d1} = 816.4$ *rad/s*; the natural frequency of the system in the second-order oscillatory link $\omega_{d2} = 221.2$ *rad/s*, and the damping ratio $\zeta_d = 0.1393$.

The bode diagram of the forward channel transfer function is the solid lines shown in Fig. 8, Fig. 9 or Fig. 10. In the normal training frequency range, the amplitude-frequency curve of the forward channel transfer function is relatively flat; the phase-frequency curve changes linearly approximately. These features provide conveniences for correcting the forward channel of CDU. In the low frequency band, the amplitude-frequency curve is flat enough, and does not need correcting. However, its phase-frequency response shows a delay property with an overall phase lag of 2°. The phase lag at 10 Hz is about 10°.

The forward channel of the CDU is a zero-type system, which cannot meet the high-order no-static-error requirement. And the dynamic performance of the loading system is poor due to the influence of the phase lag.

E. ACTIVE FORCE CONTROL STRATEGY

According to the above analysis, the hardware structure factors such as the roller's moment of inertia, the motor rotor's moment of inertia and the cable's stiffness will affect the dynamic characteristics of the forward channel. The dynamic performance of the forward channel can be improved by optimizing the structure of the CDU, but it is not significant. This approach is inflexible.

Compared with the hardware adjustment, the software compensation is flexible and easy to implement [39], [40]. The design of the active force control strategy should consider two aspects: (a) In order to improve the steady-state accuracy of the zero-type system, it is necessary to improve the system's type, so the integral correction should be introduced, but the integral correction will reduce the phase reserve of the system and affect its stability. (b) To guarantee the system's stability, the open-loop gain needs to be reduced, but the reduction will slow down the response speed. Therefore, the design of the active force control strategy should take into account the accuracy and the rapidity simultaneously. The block diagram of the active force control strategy is shown in Fig. 11.

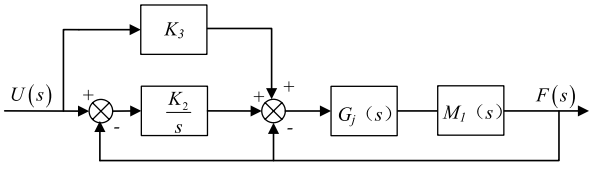

FIGURE 11. Active force control strategy.

The active force control strategy is consisted of an integral correction element, a phase lead correction element, and a feedforward correction element.

1) THE PHASE LEAD CORRECTION

In the low-frequency band, there is no need to correct the amplitude-frequency curve of the forward channel. The phase-frequency characteristic needs to be corrected to improve the phase reserve. To realize the phase lead correction, a phase-lead link $G_j(s)$ is adopted which is composed of a first order proportional and differential element and a first order inertia element.

$$G_j(s) = K_1 \frac{Ts+1}{aTs+1} \tag{8}$$

In (8), $0 < a < 1$. The first order proportional and differential element can compensate the phase lag in the middle frequency band. The first order inertia element is used to filter the high frequency noise. K_1 is used to adjust the gain of the local negative feedback, and its value is determined by the stability conditions. The frequency characteristic of the forward channel after the phase lead correction is shown in Fig. 12.

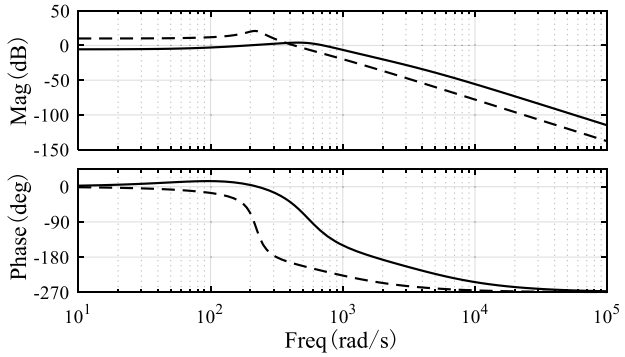

FIGURE 12. Frequency characteristic after the phase lead correction.

In Fig. 12, the solid line represents the frequency characteristic curve after the phase lead correction; the dotted line represents the frequency characteristic curve of $M_1(s)$. After the phase lead correction, there is no phase lag within 200 rad/s. It can provide sufficient phase reserve for the integral correction. The amplitude-frequency curve shows that there is a steady state error about 6 dB. The amplitude-frequency curve is still flat which facilitates the implementation of further correction.

2) THE INTEGRAL CORRECTION

In order to improve the system type and steady state accuracy, an integral link is used as the primary controller of the forward channel. The integral link improves the system from type 0 to type I. Fig. 13 shows the effect after the integral correction.

As shown in Fig. 13, the solid line represents the frequency characteristic curve after the integral correction; the dotted line represents the frequency characteristic curve of after the phase lead correction. The steady-state error of the system is obviously improved. In the premise of ensuring the loading accuracy and the stability of the system, a single integral link will decrease the phase reserve, and is not conducive to good dynamic quality.

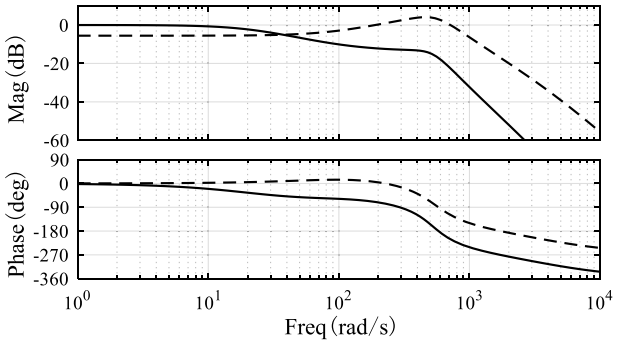

FIGURE 13. Frequency characteristic after the integral correction.

3) THE FEEDFORWARD CORRECTION

Together with the phase lead correction, the feedforward correction can improve the dynamic characteristics. In the premise of ensuring the stability, the feedforward correction is generally a proportional component. If the input signals change rapidly, the integral correction will have attenuation effect on the high frequency signals. The output of the integral correction is too small to drive the system. Owing to the feedforward link, the input signals can be input into the system directly without any intermediate links. The system is approximately in the open loop state at the moment, and the response speed of the system is improved to the utmost. When the input signals are stabilized, state, the effect of the integral correction increases, the system works under the joint action of the integral correction and the feedforward correction. The system is in closed loop state at the moment, and its steady state accuracy is guaranteed.

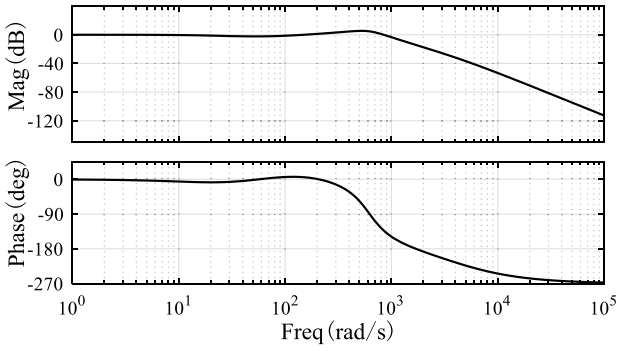

FIGURE 14. Frequency characteristic after the compound correction.

After the compound correction of the phase lead link, integral link and feedforward link, the frequency characteristic of the cable-driven force servo system is shown in Fig. 14. It can be seen from the bode diagram that the steady-state error of the corrected system is zero. The overshoot is small and the stability is good. In the range of 200 rad/s, the maximum phase lag is about 8°. The phase lag at 10 Hz is about 1.1°.

F. CONTROL EFFECT OF PID CONTROLLER

Given that the design of the CDU forward channel controller needs to balance the accuracy and speed simultaneously,

the PID controller can also be chosen. The steady-state error of the system can be reduced by the integral link in the low frequency band, and the dynamic performance is improved by the differential link in the middle frequency band. However, the differential link may amplify the feedback noise. Therefore, the incomplete differential PID controller was chosen as the forward channel controller.

$$C(s) = \frac{U(s)}{E(s)} = K_{\mathrm{p}} + \frac{K_{\mathrm{i}}}{s} + \frac{K_{\mathrm{d}} s}{\frac{s}{N} + 1} \tag{9}$$

The closed-loop frequency characteristic of the system after being corrected by the incomplete differential PID controller is the solid line shown in Fig. 15. It can be seen from the bode diagram that the steady-state error of the corrected system is zero. However, the phase lag become larger. The phase lag is approximately 25° at 10Hz (62.8 rad/s). The syntonic peak value is about 12 dB at 300rad/s.

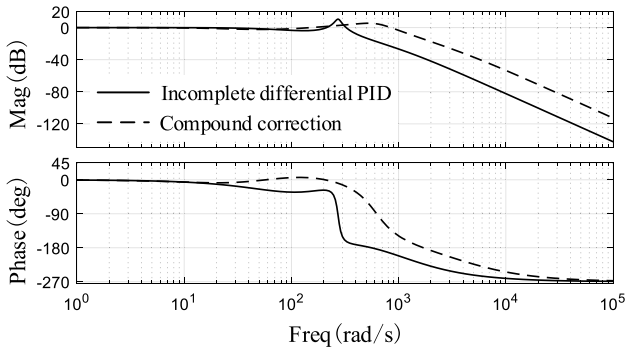

FIGURE 15. Frequency characteristic after being corrected by the incomplete differential PID controller.

To reduce the phase lag and improve the response speed, then adjust the PID controller to make the frequency characteristic optimized. However, it is discovered that the response speed and the stability are two contradictory factors. While the system gain increases, the phase lag can be reduced and the response speed can be improved, the syntonic peak value get larger at the same time which leads to poor stability. The incomplete differential PID controller can only provide limited phase compensation, leading to an unsatisfactory dynamic quality.

As can be seen in Fig. 15, compared with the incomplete differential PID controller, the compound controller can enable smaller phase lag, smaller syntonic peak value and faster response speed.

V. EXPERIMENTAL STUDY

To demonstrate the effectiveness of the proposed control strategy, the speed servo experiments and the active force servo experiments were done in this section. The cable-driven experiment platform is shown in Fig. 16. The core of the experiment platform is the LINKS semi-physical simulation platform. The construction and debugging of the controller are all completed on LINKS.

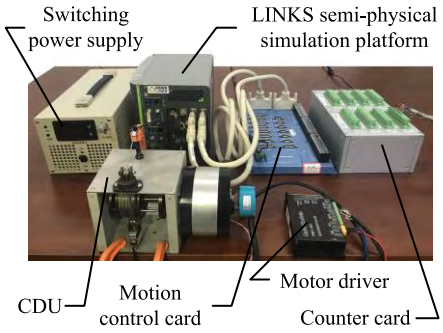

FIGURE 16. Cable-driven experiment platform.

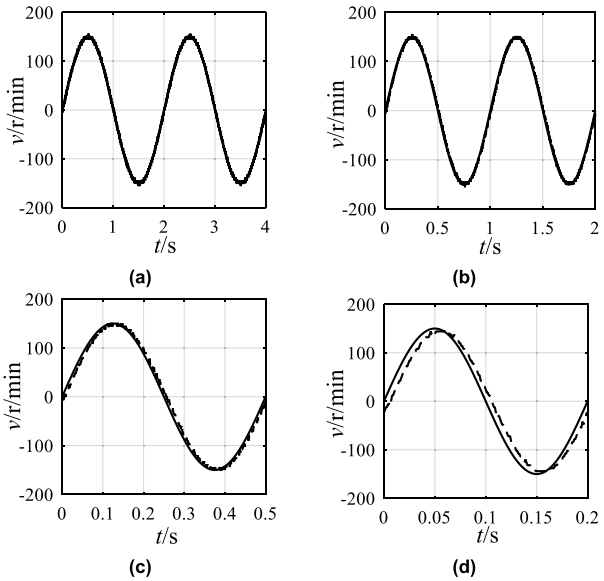

FIGURE 17. Results of the peed servo control experiments. (a) 0.5 Hz. (b) 1.0 Hz. (c) 2.0 Hz. (d) 5.0 Hz.

A. SPEED SERVO EXPERIMENTS

During the speed servo experiments, the end of the cable, hanging with 3 Kg weight, can move up and down freely. The experiments results are shown in Fig. 17. The solid line represents the desired speed curves; the dotted line represents the actual speed curves. The amplitudes of the desired speed curves are 150 r/min and the frequencies are 0.5 Hz, 1 Hz, 2 Hz and 5 Hz respectively.

The experimental results show that when the frequency of the desired speed is within 2 Hz, the cable-driven speed servo system has good tracking performance; when the frequency is 5 Hz, the actual speed has a slight phase lag (about 11°) and amplitude attenuation (about 5.6%). Considering that the rehabilitation motion of the human body is relatively gentle and the motion frequency won't be very high, the speed controller can meet the requirements of the passive rehabilitation.

B. ACTIVE FORCE SERVO EXPERIMENTS

As can be seen from Fig. 18, during the active force servo experiments, the cable's end is fixed on the fixed clip. In the

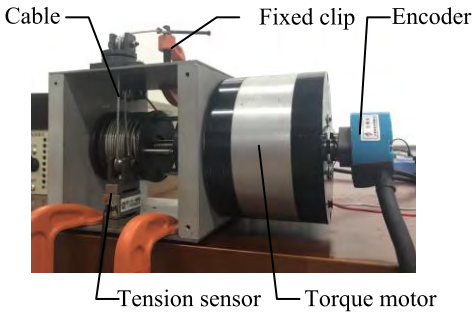

FIGURE 18. Active force servo experiments platform.

normal working process, the cable must be in the tensional state. Therefore, a 50 N pre-tightening force is loaded on the cable before the active loading. A sinusoidal force is further added on the pre-tightening force during the active loading experiments.

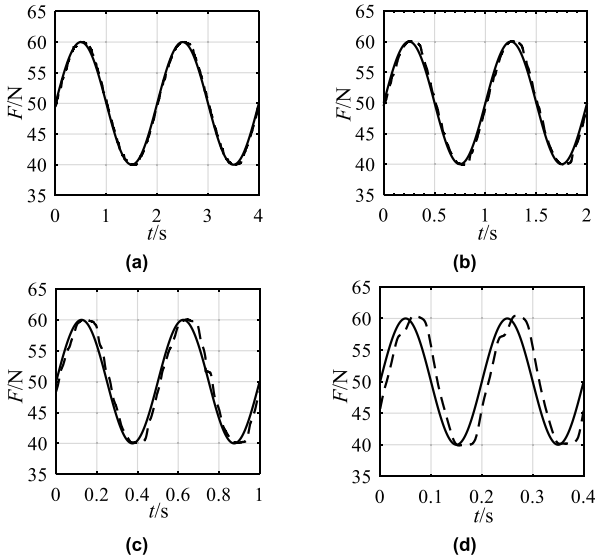

FIGURE 19. Results of the force servo control experiments. (a) 0.5 Hz. (b) 1.0 Hz. (c) 2.0 Hz. (d) 5.0 Hz.

The active loading effects based on the active force control strategy are shown in Fig. 19. The solid line represents the expected force curves; the dotted line represents the actual force curves. The amplitudes of the expected sinusoidal force curves are 10 N and the frequencies are 0.5 Hz, 1 Hz, 2 Hz and 5 Hz respectively.

The experimental results show that when the frequency is 0.5 Hz and 1 Hz, the difference between the actual force and the expected force is very small, the cable-driven force servo system has good tracking performance. When the frequency of the expected force is 2 Hz, the phase lag of the actual force is about 6°; when the frequency of the expected force is 5 Hz, the phase lag is about 20°. The differences between the actual control effects and the theoretical analysis results are mainly caused by nonlinear and uncertainty of CDU's dynamical model. However, since the patient's active movement during the initiative rehabilitation is not very intense, the active force control strategy can meet the requirements of the normal lower limb rehabilitation.

VI. CONCLUSION AND FUTRUE WORK

Aiming at the problems of the existing lower limb rehabilitation robots, a movable cable-driven lower limb rehabilitation robot has been proposed in this paper, which can realize gait training and walking training in initiative mode, passive mode and assistive mode. It has reference significance for the research of flexible medical rehabilitation equipment.

The structure composition and the realization principle of MCLR and the CDU are introduced, and the traction type and the position of the traction points are optimized according to the workspace of the robot. Based on the analysis of the cable-driven passive force servo syste, the dynamic model of the CDU is established and the active force control strategy is proposed. The validity of the active force control strategy is verified by the simulation. Furthermore, the result of speed servo experiments and active force servo experiments show that both the speed controller and the active force controller can meet the rehabilitation requirements.

The future work will further verify the accuracy of the cable-driven dynamic model. To improve the effect of the passive loading, the redundant force transfer function $M_2(s)$ will be studied and the passive force control strategy will be designed. To make full preparations for the human-machine experiments, the stability of the control system and the safety measures will be further improved.

REFERENCES

[1] J. M. Ortman, V. A. Velkoff, and H. Hogan, "An aging nation: The older population in the United States," Current Population Rep., U.S. Census Bureau, Washington, DC, USA, Tech. Rep. P25Ű1140, 2014.

[2] M. L. Bacci, *A Concise History of World Population*. Hoboken, NJ, USA: Wiley, 2017.

[3] E. Kanasi, S. Ayilavarapu, and J. Jones, "The aging population: Demographics and the biology of aging," *Periodontology*, vol. 72, no. 1, pp. 13–18, 2016.

[4] A. Basteris *et al.*, "Training modalities in robot-mediated upper limb rehabilitation in stroke: A framework for classification based on a systematic review," *J. Neuroeng. Rehabil.*, vol. 11, p. 111, Jul. 2014.

[5] W. H. Chang and Y.-H. Kim, "Robot-assisted therapy in stroke rehabilitation," *J. Stroke*, vol. 15, no. 3, pp. 174–181, 2013.

[6] W. Meng, Q. Liu, Z. Zhou, Q. Ai, B. Sheng, and S. S. Xie, "Recent development of mechanisms and control strategies for robot-assisted lower limb rehabilitation," *Mechatronics*, vol. 31, pp. 132–145, Apr. 2015.

[7] K. Y. Nam, H. J. Kim, B. S. Kwon, J.-W. Park, H. J. Lee, and A. Yoo, "Robot-assisted gait training (Lokomat) improves walking function and activity in people with spinal cord injury: A systematic review," *J. Neuroeng. Rehabil.*, vol. 14, no. 1, p. 24, 2017.

[8] E. Andrenelli *et al.*, "Improving gait function and sensorimotor brain plasticity through robotic gait training with G-EO system in Parkinson's disease," *Ann. Phys. Rehabil. Med.*, vol. 61, pp. e79–e80, Jul. 2018.

[9] A. Rathore, M. Wilcox, D. Z. M. Ramirez, R. Loureiro, and T. Carlson, "Quantifying the human-robot interaction forces between a lower limb exoskeleton and healthy users," in *Proc. IEEE 38th Annu. Int. Conf. Eng. Med. Biol. Soc. (EMBC)*, Aug. 2016, pp. 586–589.

[10] S.-H. Chen *et al.*, "Assistive control system for upper limb rehabilitation robot," *IEEE Trans. Neural Syst. Rehabil. Eng.*, vol. 24, no. 11, pp. 1199–1209, Nov. 2016.

[11] B. Ugurlu, M. Nishimura, K. Hyodo, M. Kawanishi, and T. Narikiyo, "Proof of concept for robot-aided upper limb rehabilitation using disturbance observers," *IEEE Trans. Human-Mach. Syst.*, vol. 45, no. 1, pp. 110–118, Feb. 2015.

[12] S. K. Mustafa, W. B. Lim, G. Yang, S. H. Yeo, W. Lin, and S. K. Agrawal, "Cable-driven robots," in *Handbook of Manufacturing Engineering and Technology*. London, U.K.: Springer, 2013, pp. 1–52.

[13] Y. Mao, X. Jin, G. G. Dutta, J. P. Scholz, and S. K. Agrawal, "Human movement training with a cable driven ARm EXoskeleton (CAREX)," *IEEE Trans. Neural Syst. Rehabil. Eng.*, vol. 23, no. 1, pp. 84–92, Jan. 2015.

[14] X. Jin, X. Cui, and S. K. Agrawal, "Design of a cable-driven active leg exoskeleton (C-ALEX) and gait training experiments with human subjects," in *Proc. IEEE Int. Conf. Robot. Autom. (ICRA)*, May 2015, pp. 5578–5583.

[15] G. Rosati, S. Masiero, and A. Rossi, "On the use of cable-driven robots in early inpatient stroke rehabilitation," in *Advances in Italian Mechanism Science*. Cham, Switzerland: Springer, 2017, pp. 551–558.

[16] G. Rosati, P. Gallina, S. Masiero, and A. Rossi, "Design of a new 5 d.o.f. wire-based robot for rehabilitation," in *Proc. 9th IEEE Int. Conf. Rehabil. Robot. (ICORR)*, Jun./Jul. 2005, pp. 430–433.

[17] D. Surdilovic, J. Zhang, and R. Bernhardt, "STRING-MAN: Wire-robot technology for safe, flexible and human-friendly gait rehabilitation," in *Proc. IEEE 10th Int. Conf. Rehabil. Robot.*, Jun. 2007, pp. 446–453.

[18] A. Alamdari and V. Krovi, "Design and analysis of a cable-driven articulated rehabilitation system for gait training," *J. Mech. Robot.*, vol. 8, no. 5, p. 051018, 2016.

[19] A. Alamdari and V. Krovi, "Parallel articulated-cable exercise robot (PACER): Novel home-based cable-driven parallel platform robot for upper limb neuro-rehabilitation," in *Proc. ASME Int. Design Eng. Tech. Conf. Comput. Inf. Eng. Conf.* New York, NY, USA: American Society of Mechanical Engineers, 2015, p. V05AT08A031.

[20] C. Gosselin, "Cable-driven parallel mechanisms: State of the art and perspectives," *Mech. Eng. Rev.*, vol. 1, no. 1, p. DSM0004, 2014.

[21] X. Tang, "An overview of the development for cable-driven parallel manipulator," *Adv. Mech. Eng.*, vol. 6, p. 823028, Jan. 2014.

[22] D. Chen, Y. Zhang, and S. Li, "Zeroing neural-dynamics approach and its robust and rapid solution for parallel robot manipulators against superposition of multiple disturbances," *Neurocomputing*, vol. 275, pp. 845–858, Jan. 2018.

[23] D. Chen, Y. Zhang, and S. Li, "Tracking control of robot manipulators with unknown models: A Jacobian-matrix-adaption method," *IEEE Trans. Ind. Informat.*, vol. 14, no. 7, pp. 3044–3053, Jul. 2018.

[24] R. Babaghasabha, M. A. Khosravi, and H. D. Taghirad, "Adaptive robust control of fully-constrained cable driven parallel robots," *Mechatronics*, vol. 25, pp. 27–36, Feb. 2015.

[25] D. Chen and Y. Zhang, "Robust zeroing neural-dynamics and its time-varying disturbances suppression model applied to mobile robot manipulators," *IEEE Trans. Neural Netw. Learn. Syst.*, vol. 29, no. 9, pp. 4385–4397, Sep. 2018.

[26] D. Chen and Y. Zhang, "A hybrid multi-objective scheme applied to redundant robot manipulators," *IEEE Trans. Autom. Sci. Eng.*, vol. 14, no. 3, pp. 1337–1350, Jul. 2017.

[27] D. Chen and Y. Zhang, "Minimum jerk norm scheme applied to obstacle avoidance of redundant robot arm with jerk bounded and feedback control," *IET Control Theory Appl.*, vol. 10, no. 15, pp. 1896–1903, Jun. 2016.

[28] S. Li, Y. Zhang, and L. Jin, "Kinematic control of redundant manipulators using neural networks," *IEEE Trans. Neural Netw. Learn. Syst.*, vol. 28, no. 10, pp. 2243–2254, Oct. 2016.

[29] R. Yuan, J. Luo, Z. Wu, and K. Zhao, "Study on passive torque servo system based on H_∞ robust controller," in *Proc. IEEE Int. Conf. Robot. Biomimetics (ROBIO)*, Dec. 2006, pp. 369–373.

[30] Z.-S. Ni and M.-Y. Wang, "A novel method for restraining the redundancy torque based on DFNN," *J. Harbin Inst. Technol.*, vol. 44, no. 10, pp. 47–49, 2012.

[31] B. Yang and H. Han, "A CMAC-PD compound torque controller with fast learning capacity and improved output smoothness for electric load simulator," *Int. J. Control, Autom. Syst.*, vol. 12, no. 4, pp. 805–812, 2014.

[32] X. Jiang and S. Li, "Plume front tracking in unknown environments by estimation and control," *IEEE Trans. Ind. Informat.*, to be published.

[33] W. Chengwen, J. Zongxia, S. Yaoxing, and W. Zeng, "Suppress surplus torque based on velocity closed-loop synchronization," in *Proc. IEEE Int. Conf. Fluid Power Mechatronics (FPM)*, Aug. 2011, pp. 435–439.

[34] Q. Fang, Y. Yao, and X.-C. Wang, "Disturbance observer design for electric aerodynamic load simulator," in *Proc. IEEE Int. Conf. Mach. Learn*, vol. 2, Aug. 2005, pp. 1316–1321.

[35] J. Yao, Z. Jiao, B. Yao, Y. Shang, and W. Dong, "Nonlinear adaptive robust force control of hydraulic load simulator," *Chin. J. Aeronaut.*, vol. 25, no. 5, pp. 766–775, 2012.

[36] D. Q. Truong and K. K. Ahn, "Force control for hydraulic load simulator using self-tuning grey predictor—Fuzzy PID," *Mechatronics*, vol. 19, no. 2, pp. 233–246, 2009.

[37] Q. Xiusheng, L. Jun, and L. Pengfei, "Research on electric loading simulator based on CMAC and PID compound control," *Comput. Meas. Control*, vol. 23, no. 11, pp. 3674–3676, 2015.

[38] Y. Zou, L. Zhang, L. Li, H. Ma, and K. Liu, "Running experimental research of a wire driven astronaut rehabilitative training robot," *IEEE Access*, vol. 6, pp. 11464–11471, 2018.

[39] X. Lin and R. Zhang, "H_∞ control for stochastic systems with Poisson jumps," *J. Syst. Sci. Complex.*, vol. 24, no. 4, pp. 683–700, 2011.

[40] C. W. Wang, Z. X. Jiao, and L. Quan, "Adaptive velocity synchronization compound control of electro-hydraulic load simulator," *Aerosp. Sci. Technol.*, vol. 42, pp. 309–321, Apr./May 2015.

YUPENG ZOU received the B.S. and Ph.D. degrees from the College of Mechanical and Electrical Engineering, Harbin Engineering University, in 2009 and 2014, respectively. He is currently a Lecturer with the College of Mechanical and Electrical Engineering, China University of Petroleum. His research interests mainly include rehabilitation robot and cable driven robot.

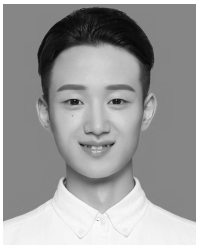

NUO WANG received the B.S. degree in vehicle engineering from the China University of Petroleum, in 2018, where he is currently pursuing the M.S. degree in mechanical engineering. His research interests include cable driven robot and control system design.

XINQING WANG received the B.S. and Ph.D. degrees from the College of Mechanical and Electrical Engineering, Harbin Institute of Technology, in 2007 and 2012, respectively. He is currently an Associate Professor with the College of Mechanical and Electrical Engineering, China University of Petroleum. His research interests include cooperative manipulator and impedance control.

HUIZI MA received the B.S. and Ph.D. degrees from the School of Economics and Management, Harbin Engineering University, in 2009 and 2014, respectively. She is currently a Lecturer with the College of Mathematics and System Science, Shandong University of Science and Technology. Her research interests mainly include stochastic control and backward stochastic differential equations.

KAI LIU received the B.S. degree in mechanical and electrical engineering from Shandong Agricultural University in 2014. He is currently pursuing the M.S. degree in mechanical engineering with the China University of Petroleum. His research interests include cable driven robot and control system design.